Real-time mass spectrometric characterization of the solid–electrolyte interphase of a lithium-ion battery

Yufan Zhou [1,2], Mao Su [3,4,5], Xiaofei Yu [1,2], Yanyan Zhang [1], Jun-Gang Wang [1], Xiaodi Ren [6], Ruiguo Cao [6], Wu Xu [6], Donald R. Baer [1], Yingge Du [3], Oleg Borodin [7,8], Yanting Wang [4,5], Xue-Lin Wang [2], Kang Xu [7,8]*, Zhijie Xu [3]*, Chongmin Wang [1]* and Zihua Zhu [1]*

The solid–electrolyte interphase (SEI) dictates the performance of most batteries, but the understanding of its chemistry and structure is limited by the lack of in situ experimental tools. In this work, we present a dynamic picture of the SEI formation in lithium-ion batteries using in operando liquid secondary ion mass spectrometry in combination with molecular dynamics simulations. We find that before any interphasial chemistry occurs (during the initial charging), an electric double layer forms at the electrode/electrolyte interface due to the self-assembly of solvent molecules. The formation of the double layer is directed by Li^+ and the electrode surface potential. The structure of this double layer predicts the eventual interphasial chemistry; in particular, the negatively charged electrode surface repels salt anions from the inner layer and results in an inner SEI that is thin, dense and inorganic in nature. It is this dense layer that is responsible for conducting Li^+ and insulating electrons, the main functions of the SEI. An electrolyte-permeable and organic-rich outer layer appears after the formation of the inner layer. In the presence of a highly concentrated, fluoride-rich electrolyte, the inner SEI layer has an elevated concentration of LiF due to the presence of anions in the double layer. These real-time nanoscale observations will be helpful in engineering better interphases for future batteries.

ithium-ion batteries (LIBs) operate on the basis of topotactic intercalation/deintercalation of Li^+ into or from the host electrode materials, during which the electrolyte should remain electrochemically inert. However, as the electrodes operate at extreme potentials far away from the thermodynamic stability limits of electrolyte components, such inertness could only be established through kinetic protection[1]. This kinetic protection is especially important for the anode because its potential (~0–0.1 V versus Li) resides well below the reduction limits of most electrolyte solvents and salt anions. Thus, in the very first charging process, trace amounts of electrolyte components decompose sacrificially to form a so-called solid–electrolyte interphase (SEI) on the anode surface[2], which functions both as a Li^+ conductor and an electronic insulator, and prevents sustained electrolyte decomposition during the subsequent cycles[2,3]. The chemical, morphological and mechanical properties of such interphases predetermine a series of key properties of LIBs, which include accessible capacity, cycling stability, rate capability and safety over the course of the battery lifetime[4–6]. In the past three decades, the SEI has been intensively investigated[3]; however, it remains "the least understood component" in LIBs[7], mainly due to the absence of an ideal analytical probe that should possess a high spatial resolution for the SEI's nanometric presence, a high temporal resolution for its evolution with electrode potential and compositional accuracy for its complicated chemistry, as well as

in situ and non-invasive natures to minimize the artefacts induced by the exposure to ambient conditions[2,3,7]. As the most advanced analytical techniques applied thus far, even cryogenic transmission electron microscopy, although it reveals important SEI structural and chemical information, still falls short of providing the dynamic evolution of the SEI under operando conditions[8,9].

The most challenging part about SEI formation is the interfacial chemical dynamics during the very first charging–discharging process. It has been proposed that, on initial charging, solvated Li^+ ions approach the surface of the negatively charged anode, whereas anions are repelled by the applied negative potential[1,10]. Such a rearrangement of the solvated cations and anions and their enrichment or depletion would constitute an electric double layer at the anode/electrolyte interface[11], whose existence should precede the reductive decomposition of any electrolyte component and SEI formation[12,13]. Theoretically, the structure and composition of this double layer should be expected to exert a significant influence on the upcoming interphase, determining how and which electrolyte component contributes to the eventual chemistry of SEI, and how durable such an interphase would be during the LIB operation. However, so far the experimental proof of such a double layer is still absent, and its link to interphasial chemistry remains a hypothesis[12,14]. To establish such a link experimentally requires an operando characterization tool that can provide accurate dynamic molecular information of the

[1]Environmental Molecular Sciences Laboratory, Pacific Northwest National Laboratory, Richland, WA, USA. [2]Institute of Frontier and Interdisciplinarity Science and Key Laboratory of Particle Physics and Particle Irradiation (MOE), Shandong University, Qingdao, China. [3]Physical and Computational Sciences Directorate, Pacific Northwest National Laboratory, Richland, WA, USA. [4]CAS Key Laboratory of Theoretical Physics, Institute of Theoretical Physics, Chinese Academy of Sciences, Beijing, China. [5]School of Physical Sciences, University of Chinese Academy of Sciences, Beijing, China. [6]Energy and Environmental Directorate, Pacific Northwest National Laboratory, Richland, WA, USA. [7]Energy & Biotechnology Division, Sensor and Electron Devices Directorate, US Army Research Laboratory, Adelphi, MD, USA. [8]Joint Center for Energy Storage Research, US Army Research Laboratory, Adelphi, MD, USA. *e-mail: conrad.k.xu.civ@mail.mil; zhijie.xu@pnnl.gov; chongmin.wang@pnnl.gov; zihua.zhu@pnnl.gov
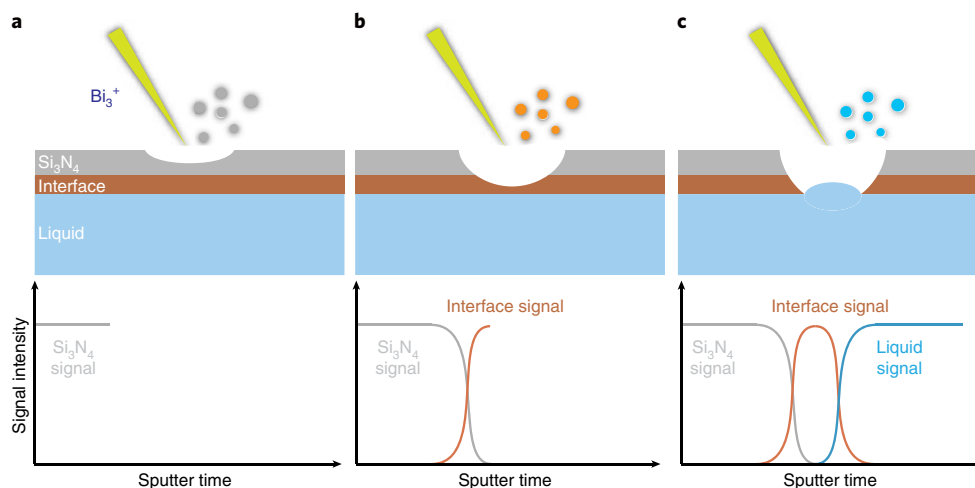
Fig. 1 | A schematic illustration of in situ liquid-SIMS analysis of solid-liquid interface. a, The liquid was separated from a high vacuum using a thin silicon nitride (in brief, Si_3N_4) membrane. At the initial stage of the SIMS analysis, only Si_3N_4-related signals were detected. **b**, Interfacial signals start to appear after a Bi_3^+ primary ion beam drills through the Si_3N_4 membrane. **c**, The liquid signals were detected after the primary ion beam drills through the interfacial layer. Note that the primary ion beam cannot drill into the liquid due to the liquid's high mobility. The surface tension can hold the liquid in the cell without any spraying out if the diameter of the aperture is reasonably small (for example, $2\,\mu m$). Also, owing to the small size of the aperture, liquid evaporation is not a problem even for high-vacuum instruments, for example, SIMS.

complicated processes that occur at electrode/electrolyte interfaces. In situ studies based on transmission electron microscopy[15–17] and atomic force microscopy[18,19] reveal vivid morphological changes of the SEI layer, with little molecular information. In situ X-ray photoelectron spectroscopy[20], X-ray diffraction[21,22] and nuclear magnetic resonance spectroscopy[23] provide accurate chemical and physical information, but at the expense of spatial resolution, which excludes the possibility of directly linking chemical information exclusively with the electrode/electrolyte interface.

In this work, we used a newly developed in situ liquid secondary ion mass spectrometry (liquid-SIMS) technique[10,24,25] (Fig. 1 and Supplementary Fig. 1) for such a purpose. The real-time formation of SEI at a copper electrode surface was monitored in an electrolyte that consisted of lithium bis(fluorosulfonyl)imide (LiFSI) dissolved in 1,2-dimethoxyethane (DME) at concentrations that ranged from dilute ($1.0\,M$) to highly concentrated ($4.0\,M$) regimes. The LiFSI–DME system was selected because a superconcentration can be readily achieved therein, which brings multiple transport and interfacial benefits that have been demonstrated to be promising for both Li-ion and Li-metal batteries[26]. The dynamic chemical mapping of the interfacial/interphasial species was thus constructed based on the chemical information collected by the liquid-SIMS, which constantly bombards the back of the Cu electrode and generates fragments for the mass spectrometer. In combination with molecular dynamics (MD) simulations, we convincingly reveal that an electric double layer indeed forms, even when the electrolyte is highly concentrated. The cation–anion separation in the double layer leads to fine structural and chemical variations of the SEI, which feature the formation of a thin and dense inner layer, which is spatially adjacent to the electrode substrate, chemically depleted in LiF and serves as an electronic insulator and Li$^+$ conductor. On top of this thin and compact layer is an organic-enriched outer layer, which is adjacent to the electrolyte and is highly permeable to the latter.

Interfacial electric double layer

The in situ electrochemical cell was constructed on a lithiated cathode ($LiCoO_2$), which serves as the counter electrode/lithium source, and a porous Cu substrate as the working electrode. A fresh cell has an open-circuit potential (OCP) close to $0\,V$, and while charging the cell removes Li$^+$ from $LiCoO_2$ and negatively polarizes the Cu electrode. It is expected that within certain potentials the electrolyte components are still thermodynamically stable, and their assembly at the Cu surface is purely 'interfacial' and no chemical change occurs; only after the applied cell voltage crosses a certain threshold will the process become 'interphasial', in which irreversible chemical decompositions of the electrolyte components occur, with the formation of SEI. During the entire charging process, the incoming ion beam mills the back of the Cu electrode (Supplementary Fig. 2) to generate depth profiles (Fig. 2) and three-dimensional (3D) ion maps (Fig. 3) to show a real-time evolution of chemical species at the Cu/electrolyte interface (Fig. 1).

The chemical mapping derived from liquid-SIMS clearly indicates that, on initial charging, the structure and chemical composition at the solid/liquid interface evolved in accordance with the potential applied to the electrode. When the cell was charged to $1\,V$, an electrical double layer was established at the solid/liquid interface, as demonstrated by the profiles of both the positive and negative ions. The negative ion depth profiles demonstrate that, when compared with those of the fresh cell (Fig. 2a), the FSI$^-$ concentration steadily decreased with an increasing of Li$^+$ concentration (Fig. 2b). Apparently, when a negative potential is applied, Li$^+$ is preferentially attracted to the vicinity of the electrode surface and FSI$^-$ ions are displaced, and so a Li$^+$-rich but anion-depleted inner-Helmholtz layer is formed. As Li$^+$ is typically solvated by solvent molecules, the presence of DME in such an electrical double layer should be proportionate to the presence of Li$^+$. Meanwhile, the apparent thickness of the Cu layer decreases (Fig. 2a,b); a plausible explanation is that a porous Cu thin electrode[10] was used in this work and the attraction force between the negative charges on the Cu electrode and the solvated Li$^+$ promoted the Li$^+$-enriched electrolyte diffusion into the porous electrode(Supplementary Figs. 3 and 4).

The formation of an electric double layer is also confirmed by the $[Li+DME]^+/Li^+$ ratio, which slightly increased after applying a $1.0\,V$ potential (Fig. 2a,b), which indicates that more solvated Li$^+$ ions aggregate at the electrode/electrolyte interface. A further increase in Li$^-$ and decrease of FSI$^-$ occur when the cell is charged to $2.0\,V$ (Fig. 2c), which suggests that the separation of Li$^+$ and FSI$^-$ becomes more significant with the negative polarization of the Cu electrode.
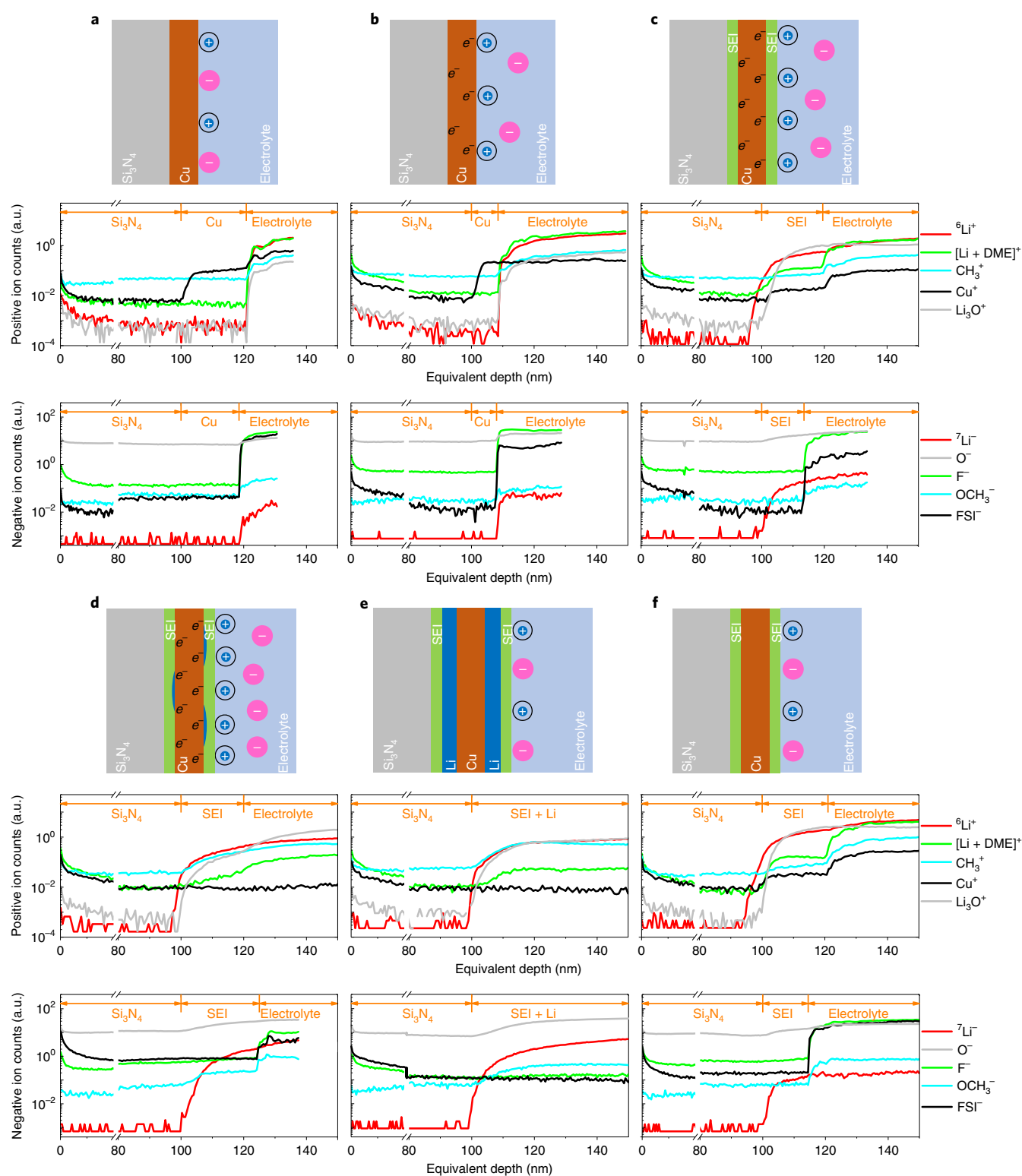
Fig. 2 | A schematic illustration of the formation of an SEI layer at the Cu anode surface with 1.0 M LiFSI in DME as the electrolyte and the corresponding positive ion and negative ion SIMS depth profiles. a–f, Top rows: a fresh cell, OCP, both anions (FSI⁻) and cations (solvated Li⁺ ions) can stay on the Cu electrode surface (**a**); at 1.0 V, an electrical double layer forms and the electric force attracts solvated Li⁺ ions, which leads to a better wettability of the electrolyte on the Cu surface (**b**); at 2.0 V, the inner SEI layer forms at the electrode/electrolyte interface, which includes the back side of the Cu electrode, because a porous Cu electrode is used[10] (**c**); at 3.0 V, a small amount of Li metal may already be deposited on the Cu electrode surface (more discussions is given in the Supplementary Information) (**d**); after charging, a larger amount of Li metal forms at both sides of the Cu electrode (**e**); after discharging, Li metal is stripped off and only the SEI layer attaches on the Cu surface (**f**). It is of great interest to observe that SEI and Li metal layers can form between the Cu electrode and the Si₃N₄ membrane. More discussions about this observation are given in Supplementary Information. The middle rows in **a–f** correspond to the positive ion depth profiles and the bottom rows in **a–f** correspond to the negative ion depth profiles. a.u., arbitrary units.
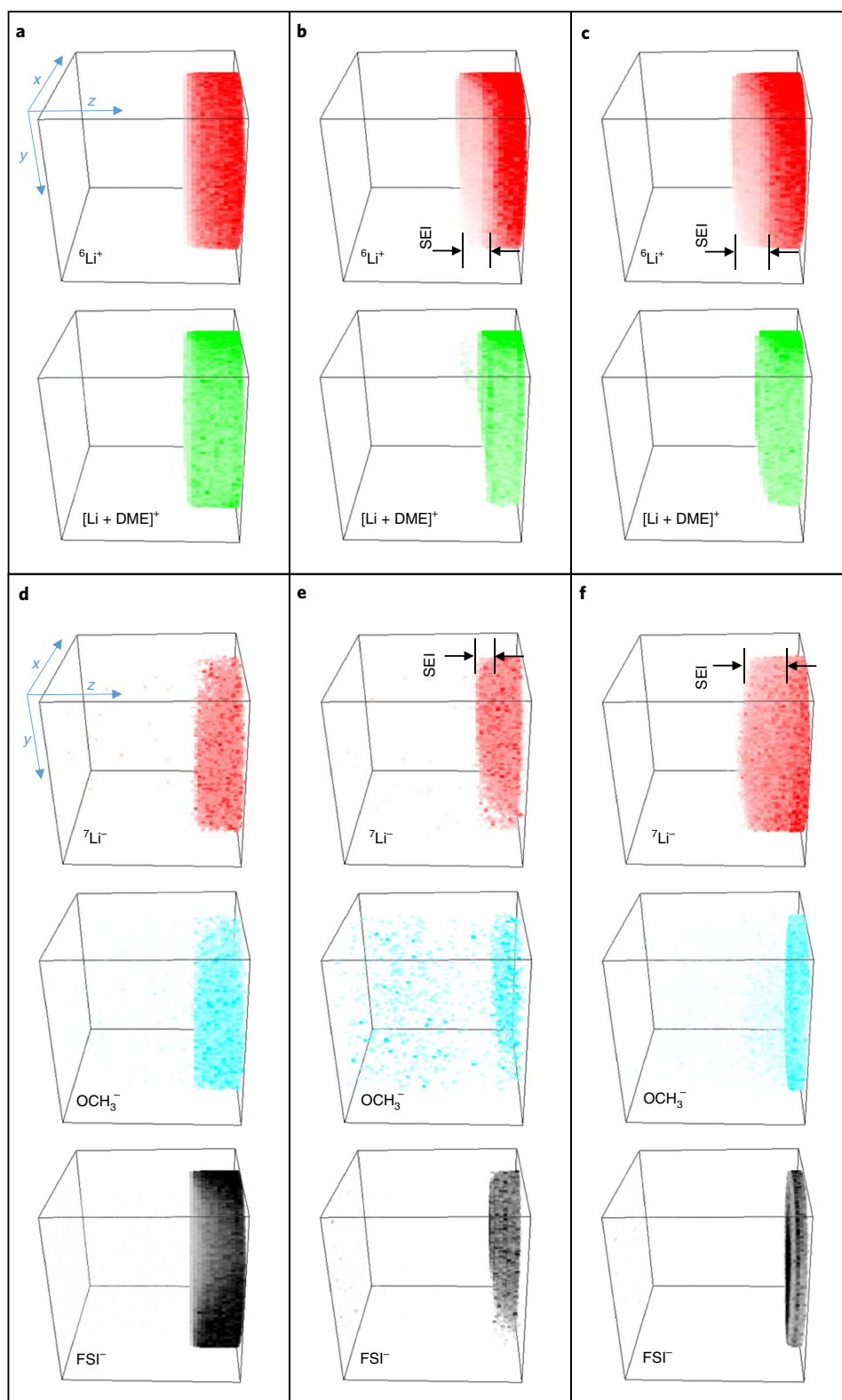
Fig. 3 | 3D maps of important secondary ion species. The ion maps were reconstructed from the raw liquid-SIMS data. **a–c**, $^6Li^+$ and $[Li+DME]^+$ maps at fresh OCP state (**a**), charging to 2.0 V (**b**) and discharged OCP state (**c**). At the fresh state, $^6Li^+$ and $[Li+DME]^+$ ions appear simultaneously when liquid electrolyte is exposed. As a comparison, when charging at 2.0 V, $^6Li^+$ appears before $[Li+DME]^+$, which suggests a Li-contained solid layer (inner SEI) forms. After discharge, the result is very similar with the 2.0 V situation, which suggests that the inner SEI layer is not dissolved after discharging. **d–f**, $^7Li^-$, OCH_3^- and FSI^- maps at fresh OCP state (**d**), charging to 2.0 V (**e**) and discharged OCP state (**f**). At the fresh state, the $^7Li^-$, OCH_3^- and FSI^- ions appear simultaneously when liquid electrolyte is exposed, consistent with the positive ion result. Also, at the 2.0 V state, the $^7Li^-$ signal appears earlier than the OCH_3^- and FSI^- signals, which suggests that a Li-contained solid layer (inner SEI) forms. The ion maps after discharging are similar to the 2.0 V data; however, the OCH_3^- signal becomes much strong after discharging, which suggests the formation of an organic-enriched layer (outer SEI layer) besides the inner SEI layer.

- Cu   Li$^+$ FSI$^-$ DME
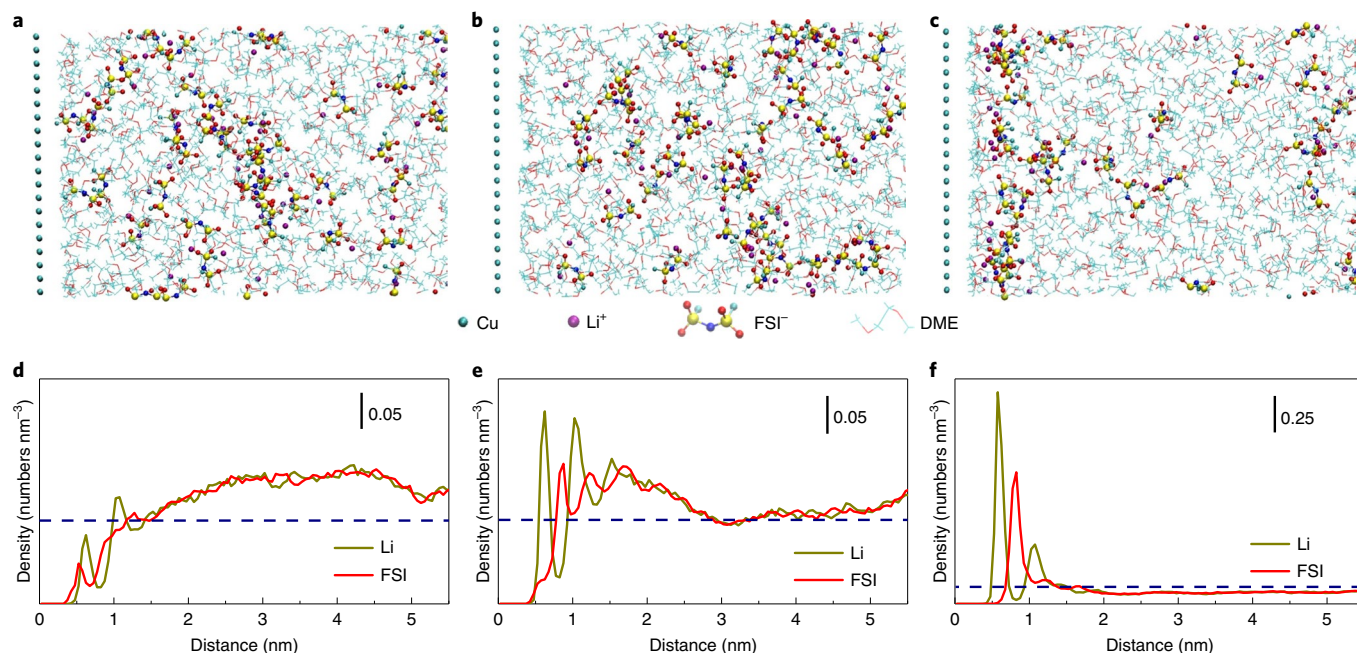
Fig. 4 | Simulation snapshots and line plots of the ion distribution near to a Cu electrode and a 1.0 M LiFSI in DME electrolyte interface with increasing voltage. a–c, Snapshots (top) from the simulation at 0 V (**a**), 1.0 V (**b**) and 2.8 V (**c**). A Cu electrode is shown on the left in **a**, **b** and **c**. The ion distributions near to the anode are shown in 0 V (**d**), 1.0 V (**e**) and 2.8 V (**f**). When no potential was applied, no Li$^+$ enrichment at the electrode/electrolyte interface was observed, as shown in **d**. As a comparison, a Li$^+$-enriched layer formed at the electrode/electrolyte interface when negative potentials were applied on the Cu electrode, as shown in **e** and **f**. **e** and **f** also suggest that the thickness of the electric double layer seems to be less than 1 nm. A comparison of **e** and **f** suggests that the Li$^+$ enrichment at the electrode/electrolyte interface becomes more significant when a higher potential is applied. The dashed lines in **d**–**f** indicate an even distribution.

The above experimental observation on the formation of an electric double layer is well corroborated by MD simulation of a 1.0 M LiFSI–DME mixture at a negatively charged surface. At OCP, neither Li$^+$ nor FSI$^-$ dominates the electrode/electrolyte interface (Fig. 4a,d). When a 1.0 V charge is applied, a Li$^+$-enriched layer of ~0.6 nm appears at the electrode/electrolyte interface (Fig. 4e), which is adjacent to an FSI$^-$-enriched layer of ~0.8 nm close to the liquid (Fig. 4e). When a higher potential is applied, Li$^+$ enrichment at the electrode/electrolyte interface increases (Fig. 4c,f).

Interphasial chemistry and structure

When the cell potential crosses ~2 V, the electric double layer evolves to a Li-enriched but electrolyte-depleted layer (Figs. 2c and 3b,e), which is classically termed as SEI.

Traditionally, LiF is believed to be an inevitable component in the SEI[2,3,27], but its effect, beneficial or detrimental, has been controversial[28]. Recent studies attributed new cell performances to the highly LiF-rich interphases[29,30]. In most of these cases, fluorine comes from the reduction of the anion, unless the solvent molecules also bear fluorine that is available from electrochemical reduction. In the current electrolyte based on an ether solution of LiFSI, the anion reduction seems to be disfavoured by the negatively charged electrode, because the introduction of fluorinated species into SEI has to overcome the repulsion from the Cu electrode when the cell is charged above 2.0 V, as shown in Fig. 2c in which F$^-$ and FSI$^-$ signals show a negligible presence in the SEI. Apparently, prior to the formation of the SEI layer, the electric double layer depleted in anion is responsible for this low fluorinated interphase, whereas the preferred species in the inner-Helmholtz layer, solvated Li$^+$, leads to an interphase that is rich in species from the reduction of the solvent molecules. Density functional theory calculations confirm that the solvent molecules are more susceptible to reduction if they are in the primary solvation sheath of Li$^+$ (ref. [3]) and, therefore, a fluorine-depleted SEI layer would ensue in such an electrolyte. An interphase highly rich in fluorine can only occur with either a solvent molecule that also carries fluorine or when the salt anion is forced into the inner-Helmholtz layer by the high salt concentrations.

Besides chemical information, liquid-SIMS also generates reliable morphological information and reveals a well-structured SEI. Conceptually, it has been proposed that an SEI layer might consist of a dense inner layer, which is adjacent to the solid electrode and is dominated by inorganic components, and an outer layer, which is adjacent to the liquid side and is dominated by the organic components[2,31]. Such a hierarchy can be established beyond doubt by the liquid-SIMS chemical mapping, in which the C$^-$ and CH$^-$ signals remain low and constant throughout the SEI (Supplementary Fig. 5), indicating that the hydrocarbon is not a major component, and the major components of the SEI layer should be inorganic. Most probably, the SEI observed corresponds to the inner layer. Strong O$^-$ and [Li$_{2n+1}$O$_n$]$^+$ signals for this inner SEI layer suggest that the major component of the inner SEI is most probably Li$_2$O (Fig. 2c,f). The detected [Li$_n$(OH)$_{n+1}$]$^-$ ions also indicate the existence of LiOH in the SEI.

After discharging, the inner SEI is dense and impermeable to electrolyte components. For example, FSI$^-$ and F$^-$ ions do not show any clear increase in the inner SEI layer (Figs. 2f and 3f). Fundamentally, solvation of the salt anions is weak in electrolytes[3,32,33] and the size of FSI$^-$ is smaller than 1 nm. If so, the inner SEI layer should be rather dense and even small FSI$^-$ ions cannot diffuse into it.

Within the SEI layer, atop the dense layer, as described above, is an outer layer that is organic enriched and adjacent to the liquid electrolyte. This fine structural feature is supported by Fig. 3d–f and Supplementary Fig. 5f, which show that, after discharging, the C$^-$, CH$^-$ and OCH$_3^-$ signals that should originate from an organic
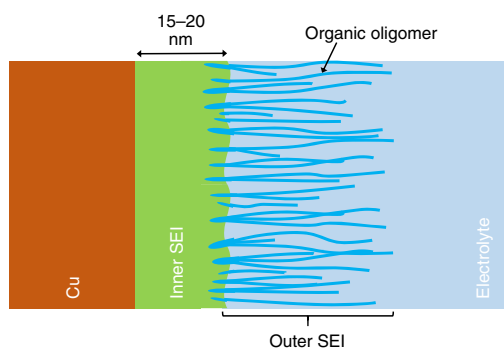
Fig. 5 | An SEI model based on the observations in this work. The SEI can be divided into two parts: an inner SEI and an outer SEI. The inner SEI is continuous, dense and impermeable to electrolytes, and it is most probably composed of Li$_2$O. The outer SEI is mainly composed of loose organic oligomers that result from the degradation of solvent molecules. The loose outer SEI is permeable to electrolytes.

entity experience a clear increase as soon as the signals for the bulk electrolyte appear. As a comparison, the signals of these species only show a limited increasing at the state of the fresh cell, or the cells after being charged to 1.0 and 2.0 V (Supplementary Fig. 5a–c). As the inner dense SEI already forms at 2.0 V, such a diffused and organic-enriched outer layer must be generated after the formation of the inner dense SEI, and consists of partially reoxidizable interphase ingredients that can be observed by using atomic force microscopy and an electrochemical quartz crystal microbalance[19]. Interestingly, both [Li+DME]$^+$ and FSI$^-$ after discharging show similar intensities to that of the fresh cell (Fig. 2a,f), which suggests that this diffused outer SEI layer is very permeable to the bulk electrolyte. The existence of this diffused outer SEI layer might act as an intermediate phase that assists in the desolvation or resolvation of Li$^+$ when Li$^+$ ions migrate into or leave from the dense part of the SEI, in which no solvent molecules are allowed, and the original solvation sheath has to be stripped away. The rich oxygen functionalities in this porous outer layer might provide sufficient coordination to Li$^+$ as a transition so that its solvation environment does not experience a sudden change from a full solvation sheath in the bulk electrolyte to an inorganic solid state with coordination sites fixed on the lattice. Otherwise, an abrupt discontinuity in the coordination environments usually comes with a steep energy barrier, which makes it difficult for Li$^+$ to complete the cycle.

A structured SEI

The observations described above firmly indicate a structured SEI that consists of two layers: a thin, inorganic and compact inner layer that is dominated by Li$_2$O but chemically depleted of LiF, and a diffuse, organic-enriched outer layer, which is permeable to liquid (Fig. 5). The SIMS profiles in Fig. 2f indicate that the thickness of the inner SEI should be about 15–20 nm, consistent with estimates from numerous ex situ measurements, such as transmission electron microscopy[34], but much thinner than that observed in many in situ methods, such as atomic force microscopy[18]. The difference between the two should reflect the diffused and porous outer layer. This 15~20 nm thickness seems to be very reasonable as it effectively separates the electrode and the bulk electrolyte, as indicated by the variation of chemical species with the sputtering depth. This thin inner layer should be responsible for preventing the electron tunnelling that usually occurs at a length scale of <2 nm, but still allow Li$^+$ to migrate through at sufficient rates. Certainly, the above thickness should only be taken as an approximate range rather than an accurate value, because the sputtering rate is based on the Si$_3$N$_4$

membrane, which may differ from that of the inorganic species in this interphase. The thickness of the outer SEI is difficult to measure using in situ liquid-SIMS, because the liquid electrolyte in this layer is mobile and cannot be drilled through by the primary ion beam[35]. However, it can be estimated from the wide range of SEI thicknesses (5–500 nm) (ref. [3]) reported in the literature, which shows a variety of methods in which the survival of such soft outer layers varies and could be responsible for the upper-limit recorded.

This structured SEI provides many needed insights that will aid in the design of a more effective interphase. Although most chemical analyses provide overall chemical information, it is vitally important to know the exact distribution of these chemicals throughout the interphase to differentiate which ingredient serves as the necessary and truly functional SEI component. One typical example is LiF, which has been frequently detected in various interphases; however, there are conflicting reports about its usefulness in rendering a protective interphase[28]. The profiles generated by liquid-SIMS reveal that, due to the negatively charged electrode surface, the only fluorine source in the electrolyte (FSI$^-$) is expelled from the inner-Helmholtz layer structure, which results in a Li$_2$O-rich but LiF-depleted interphase. Thus, the interphases formed in electrolytes that consist of non-fluorinated solvents are intrinsically fluorine free, unless additional fluorine sources, such as fluorinated solvents or additives, are present, or the electrolytes are superconcentrated such that they force salt anions (with fluorine) into the near vicinity of the electrode. This is exactly why these additional fluorine sources were employed in recent studies to enable new properties[12,14,29] that are otherwise unavailable from fluorine-depleted interphases[36–39]. We emphasize that, despite the insulating nature of LiF, recent studies identified highly fluorinated interphases as the desired interphasial chemistry, and an enhanced Li$^+$ conduction mechanism was proposed[40].

Concentration effect

Superconcentration not only alters the solvation structure of both cations and anions, but also significantly affects the inner-Helmholtz layer structure by forcing fluorinated anions into the vicinity of the electrodes. In this work, the case of a 4.0 M LiFSI–DME electrolyte was investigated. Both liquid-SIMS data (Supplementary Fig. 6b,h) and MD simulation results (Supplementary Fig. 7) support the existence of an electric double layer near the electrode surface before the formation of SEI, similar to the case of the 1.0 M electrolyte. However, the separation of Li$^+$ from FSI$^-$ is obviously much less significant (Supplementary Fig. 8).

The difference in the interfacial structure of 1.0 M and 4.0 M electrolytes is essentially reflected in their respective interphasial chemistries. An elevated fluorine concentration was observed in the SEI of the 4.0 M case; however, the fluorine concentration was still low (at most, a few percent; more details are given in Supplementary Information). Therefore, superconcentration is a less effective way to fight the fluorine depletion; instead, addition fluorinated solvents or additives that are neutral and have little repulsion from the negatively charged electrode surface are more effective in delivering fluorine to the interphase. For the recent efforts that seek a more fluorinated interphase to stabilize either Li metal or high Ni cathode surfaces, a superconcentration approach should be replaced by a fluorinated solvent approach.

Conclusions

In this work, we investigated the formation mechanism of SEI using liquid-SIMS under operando conditions. We showed that, before any interphasial chemistry occurs during the initial charging, an interfacial electric double layer forms between the electrode and the electrolyte via the self-assembly of electrolyte solvent molecules directed by Li$^+$. MD simulations visualized the detailed molecular-level structure of this electric double layer. The double layer

becomes anion depleted once the electrode is negatively charged, and the resultant interfacial structure predicts the interphasial chemistries in the electrolytes, in which a fluorine presence is intrinsically disfavoured. A superconcentrated electrolyte alleviates the fluorine depletion in the interfacial structure, but cannot reverse the dominance of solvent molecules. For aggressive battery chemistries that require highly fluorinated interphases, such as Li metal or high Ni cathodes, additional fluorine sources, such as fluorinated solvents or additives, have to be introduced. The chemical profiles established by liquid-SIMS also reveal a structured SEI, in which the inner layer is dense, inorganic but LiF-depleted, whereas the outer layer, rich in organic species, is diffuse and permeable to the bulk electrolyte. In principle, the same strategy can also be used to study the cathode–electrolyte interphase. This molecular understanding of the chemical-depth distribution in SEI will help design a better interphase for future battery chemistries.

Online content

Any methods, additional references, Nature Research reporting summaries, source data, extended data, supplementary information, acknowledgements, peer review information; details of author contributions and competing interests; and statements of data and code availability are available at https://doi.org/10.1038/s41565-019-0618-4.

References

1. Xu, K. Nonaqueous liquid electrolytes for lithium-based rechargeable batteries. *Chem. Rev.* **104**, 4303–4418 (2004).
2. Gauthier, M. et al. Electrode–electrolyte interface in Li-ion batteries: current understanding and new insights. *J. Phys. Chem. Lett.* **6**, 4653–4672 (2015).
3. Xu, K. Electrolytes and interphases in Li-ion batteries and beyond. *Chem. Rev.* **114**, 11503–11618 (2014).
4. Smith, A. J., Burns, J. C., Trussler, S. & Dahn, J. R. Precision measurements of the Coulombic efficiency of lithium-ion batteries and of electrode materials for lithium-ion batteries. *J. Electrochem. Soc.* **157**, A196–A202 (2010).
5. Shim, J., Kostecki, R., Richardson, T., Song, X. & Striebel, K. A. Electrochemical analysis for cycle performance and capacity fading of a lithium-ion battery cycled at elevated temperature. *J. Power Sources* **112**, 222–230 (2002).
6. Menkin, S., Golodnitsky, D. & Peled, E. Artificial solid-electrolyte interphase (SEI) for improved cycleability and safety of lithium-ion cells for EV applications. *Electrochem. Commun.* **11**, 1789–1791 (2009).
7. Winter, M. The solid electrolyte interphase—the most important and the least understood solid electrolyte in rechargeable Li batteries. *Z. Phys. Chem.* **223**, 1395–1406 (2009).
8. Wang, X. F. et al. New insights on the structure of electrochemically deposited lithium metal and its solid electrolyte interphases via cryogenic TEM. *Nano Lett.* **17**, 7606–7612 (2017).
9. Zachman, M. J., Tu, Z. Y., Choudhury, S., Archer, L. A. & Kourkoutis, L. F. Cryo-stem mapping of solid–liquid interfaces and dendrites in lithium-metal batteries. *Nature* **560**, 345–349 (2018).
10. Zhu, Z. et al. In situ mass spectrometric determination of molecular structural evolution at the solid electrolyte interphase in lithium-ion batteries. *Nano Lett.* **15**, 6170–6176 (2015).
11. Frackowiak, E. & Béguin, F. Carbon materials for the electrochemical storage of energy in capacitors. *Carbon* **39**, 937–950 (2001).
12. Yang, C. et al. 4.0 V aqueous Li-ion batteries. *Joule* **1**, 122–132 (2017).
13. Gourdin, G., Zheng, D., Smith, P. H. & Qu, D. In situ electrochemical–mass spectroscopic investigation of solid electrolyte interphase formation on the surface of a carbon electrode. *Electrochim. Acta* **112**, 735–746 (2013).
14. Wang, F. et al. Hybrid aqueous/non-aqueous electrolyte for safe and high-energy Li-ion batteries. *Joule* **2**, 927–937 (2018).
15. Sacci, R. L. et al. Nanoscale imaging of fundamental Li battery chemistry: solid–electrolyte interphase formation and preferential growth of lithium metal nanoclusters. *Nano Lett.* **15**, 2011–2018 (2015).
16. Leenheer, A. J., Jungjohann, K. L., Zavadil, K. R., Sullivan, J. P. & Harris, C. T. Lithium electrodeposition dynamics in aprotic electrolyte observed in situ via transmission electron microscopy. *ACS Nano* **9**, 4379–4389 (2015).
17. Mehdi, B. L. et al. Observation and quantification of nanoscale processes in lithium batteries by operando electrochemical (S)TEM. *Nano Lett.* **15**, 2168–2173 (2015).
18. Cresce, Av, Russell, S. M., Baker, D. R., Gaskell, K. J & Xu, K. In situ and quantitative characterization of solid electrolyte interphases. *Nano Lett.* **14**, 1405–1412 (2014).
19. Liu, T. C. et al. In situ quantification of interphasial chemistry in Li-ion battery. *Nat. Nanotechnol.* **14**, 50–56 (2019).
20. Oswald, S., Nikolowski, K. & Ehrenberg, H. Quasi in situ XPS investigations on intercalation mechanisms in li-ion battery materials. *Anal. Bioanal. Chem.* **393**, 1871–1877 (2009).
21. Nazri, G. & Muller, R. H. In situ X-ray diffraction of surface layers on lithium in nonaqueous electrolyte. *J. Electrochem. Soc.* **132**, 1385–1387 (1985).
22. Wagner, M. R., Albering, J. H., Moeller, K. C., Besenhard, J. O. & Winter, M. XRD evidence for the electrochemical formation of in PC-based electrolytes. *Electrochem. Commun.* **7**, 947–952 (2005).
23. Bhattacharyya, R. et al. In situ NMR observation of the formation of metallic lithium microstructures in lithium batteries. *Nat. Mater.* **9**, 504–510 (2010).
24. Zhang, Y. Y. et al. Potential-dynamic surface chemistry controls the electrocatalytic processes of ethanol oxidation on gold surfaces. *ACS Energy Lett.* **4**, 215–221 (2019).
25. Wang, J. G. et al. Direct molecular evidence of proton transfer and mass dynamics at the electrode–electrolyte interface. *J. Phys. Chem. Lett.* **10**, 251–258 (2019).
26. Qian, J. F. et al. High rate and stable cycling of lithium metal anode. *Nat. Commun.* **6**, 6362 (2015).
27. Edström, K., Herstedt, M. & Abraham, D. P. A new look at the solid electrolyte interphase on graphite anodes in Li-ion batteries. *J. Power Sources* **153**, 380–384 (2006).
28. Wang, C., Meng, Y. S. & Xu, K. Perspective—fluorinating interphases. *J. Electrochem. Soc.* **166**, A5184–A5186 (2019).
29. Suo, L. M. et al. 'Water-in-salt' electrolyte enables high-voltage aqueous lithium-ion chemistries. *Science* **350**, 938–943 (2015).
30. Fan, X. L. et al. Non-flammable electrolyte enables Li-metal batteries with aggressive cathode chemistries. *Nat. Nanotechnol.* **13**, 715–722 (2018); erratum **13**, 1191 (2018).
31. Lu, P. & Harris, S. J. Lithium transport within the solid electrolyte interphase. *Electrochem. Commun.* **13**, 1035–1037 (2011).
32. Hayamizu, K., Aihara, Y., Arai, S. & Martinez, C. G. Pulse-gradient spin-echo ^{1}H, ^{7}Li, and ^{19}F NMR diffusion and ionic conductivity measurements of 14 organic electrolytes containing LiN(SO$_2$CF$_3$)$_2$. *J. Phys. Chem. B* **103**, 519–524 (1999).
33. Cresce, A. V. et al. Anion solvation in carbonate-based electrolytes. *J. Phys. Chem. C* **119**, 27255–27264 (2015).
34. Nie, M. & Lucht, B. L. Role of lithium salt on solid electrolyte interface (SEI) formation and structure in lithium ion batteries. *J. Electrochem. Soc.* **161**, A1001–A1006 (2014).
35. Ding, Y. Z. et al. In situ molecular imaging of the biofilm and its matrix. *Anal. Chem.* **88**, 11244–11252 (2016).
36. Wang, J. et al. Superconcentrated electrolytes for a high-voltage lithium-ion battery. *Nat. Commun.* **7**, 12032 (2016).
37. Wan, C. et al. Multinuclear NMR study of the solid electrolyte interface formed in lithium metal batteries. *ACS Appl. Mater. Interface* **9**, 14741–14748 (2017).
38. Nie, M. et al. Role of solution structure in solid electrolyte interphase formation on graphite with LiPF$_6$ in propylene carbonate. *J. Phys. Chem. C* **117**, 25381–25389 (2013).
39. von Cresce, A. & Xu, K. Electrolyte additive in support of 5 V Li ion chemistry. *J. Electrochem. Soc.* **158**, A337–A342 (2011).
40. Zhang, Q. et al. Synergetic effects of inorganic components in solid electrolyte interphase on high cycle efficiency of lithium ion batteries. *Nano Lett.* **16**, 2011–2016 (2016).

Methods

Cell preparation. The battery cell was fabricated on a polyether ether ketone block using the method reported in a previous publication[10] with minor adaptations. In brief, a liquid chamber with a size of 6.0 mm (length) × 5.5 mm (width) × 1.0 mm (height) was machined on the polyether ether ketone block with two liquid channels for the introduction of the electrolytes. The Li-ion battery cathode, a $LiCoO_2$ layer (~55 μm thick) coated on a thin Al foil (~15 μm thick), was immobilized at the bottom of the liquid chamber. The anode, a ~70 nm thick Cu film, was sputter coated on a 100 nm thick Si_3N_4 membrane, which was immobilized on a silicon frame of 7.5 mm (length) × 7.5 mm (width) × 0.2 mm (height). The silicon frame (with the Si_3N_4 membrane and Cu anode below it) was placed on top of the liquid chamber and sealed using an epoxy glue. The effective cathode area was about 10.0 mm², the effective anode area was about 4.0 mm² and the distance between them was about 0.8 mm. Two thin Cu wires were attached to the cathode and anode, respectively, using Ag paste so the battery could be charged–discharged. After assembling of the cell, a desirable electrolyte (1.0 M or 4.0 M LiFSI in DME here) could be introduced into the liquid chamber in an argon-filled glove box. After being sealed, the Li-ion battery cell was loaded on a time-of-flight SIMS sample holder (Supplementary Fig. 1) and then introduced into the SIMS instrument for operando analysis.

A constant-current mode (1.5×10^{-6} A) was used for the charging and discharging in this work. A Li-ion battery cell could be charged–discharged for at least ten cycles[10]. A typical charge–discharge curve is shown in Supplementary Fig. 2. The voltage quickly (less than 30 s) increased to 1.5 V, and then gradually increased to ~3.7–3.8 V (~1,500–1,600 s) until it slightly decreased to reach a relatively stable value at 3.6 V. After further charging for 800 s, the battery was discharged to 0.5 V to make sure that most of the Li metal was stripped from the Cu anode. The in situ liquid-SIMS measurements were performed at six states— fresh cell (open circuit), charged to 1.0, 2.0 and 3.0 V, after the third charging (open circuit) and after the third discharge (open circuit), respectively (as shown in Fig. 2). For the 1.0, 2.0 and 3.0 V states, the cell potentials were held at a constant potential mode during the SIMS measurement. For example, 1.0 V was reached after about 20 s of charging, and then the potential was held at 1.0 V for the SIMS measurement. Similarly, 2.0 V was reached after about 350 s of charging, and then the potential was held at 2.0 V for the SIMS measurement; 3.0 V was reached after about 900 s of charging, and then the potential was hold at 3.0 V for the SIMS measurement. To avoid mechanical failure of the Si_3N_4 membrane, only one measurement was performed for each battery cell. At least two cells were examined for each state to ensure data repeatability.

In situ liquid-SIMS. The SIMS analysis was carried out using a time-of-flight SIMS V instrument (IONTOF GmbH). Beam damage was a serious concern in liquid-SIMS measurements, so a desirable instrument setting was critical to minimize the beam damage. The optimum instrumental setting is described in detail in a recent publication[41], and cluster primary ions must be used. In this work, a pulsed 25 kV Bi_3^+ beam of diameter ~500 nm was used for all the measurements. The pulse frequency was ~10 kHz, the pulse width was about 150 ns and the corresponding beam current was ~0.36 pA. The incident angle of the primary Bi_3^+ beam was 45° degree off the normal. For each measurement, the Bi_3^+ beam was scanned on a round area of ~2 μm in diameter around the centre of the Si_3N_4 membrane to drill a hole in it. The measurement was stopped when stable liquid signals were observed (normally 50–200 s after the liquid signals were detected). A mass spectrum, depth profiles and 2D ion images were simultaneously collected, and 3D ion maps were available after reconstruction of the raw data. Battery charging and discharging were performed in the analysis chamber and the SIMS measurement was performed simultaneously. The pressure in the analysis chamber was about 5×10^{-7} to 1×10^{-6} mbar with the sample present. During the SIMS measurements, the pressure change normally was negligible. A low-energy electron flood gun (~10 eV, 1 μA) was used for charge compensation during the measurements. Note that only unit mass resolution spectra could be obtained in this work[41], and mass interference might need to be considered in some cases.

To ensure the data reproducibility, at least two cells for each condition were tested. The SIMS depth-profile data are very reproducible for most cases, for example, fresh cell, the 1.0 V condition, the 2.0 V condition, after charging and after discharging. The sample-to-sample difference of the thickness (based on sputtering time) for each solid layer (Si_3N_4, Cu SEI) can be within ±10%. Only the 3.0 V polarization presented a challenging case, in which the thickness of the SEI + Li layer could vary by ±30% due to the on-going dynamic reaction.

Quantification using SIMS is challenging because different ion species may have different ionization yields (so-called matrix effect). However, semi-quantification, that is, sample-to-sample comparison, has been extensively used in SIMS data analysis. For example, in this work, a comparison of the 1.0 V data to the fresh-cell data shows that the FSI⁻ signal decreases along with an increasing Li⁻ signal, which suggests an increase of Li ions and a decrease of FSI at the electrode/electrolyte interface, that is, the formation of a potential-induced electric double layer.

Computer simulation details. MD simulations of the LiFSI–DME mixture were performed at 333 K for both 1.0 and 4.0 M concentrations, which correspond to 576 DME/64 LiFSI and 448 DME/320 LiFSI, respectively. A single-layer Cu(100) electrode was fixed on both sides of the simulation domain. Amber force field[42] parameters for Cu were used, with the partial charges modified for

different voltages. Voltages were calculated using the same method as shown in previous work[43]. The simulation boxes were $3.6 \times 3.6 \times 9$ nm³ for 1.0 M and $3.24 \times 3.24 \times 12.5$ nm³ for 4.0 M, with 9.0 and 12.5 nm the dimensions between the two electrodes, respectively. The two electrodes were fixed at both ends of the simulation box and perpendicular to the z axis. The simulation boxes were periodic along the x and y directions. The distances between the two electrodes were chosen such that the forces on the particles at the middle of box were statistically the same as those in the bulk simulations without electrodes. After equilibrium, a 40 ns NVT run was performed for each concentration with a sampling on the time interval of 2 ps to collect the simulation data. A many-body polarizable force field APPLE&P[44] and Gromacs[45] software were used. The atomic polarizability was neglected to accelerate simulation, which should have a negligible influence on the results[46].

Data availability

All data that support the findings of this study have been included in the main text and Supplementary Information. The original data are archived at the Environmental Molecular Sciences Laboratory at Pacific Northwest National Laboratory and are available from the corresponding authors upon reasonable request.

Code availability

The original code for MD simulation is kept at the Environmental Molecular Sciences Laboratory at Pacific Northwest National Laboratory and is available from the corresponding authors upon reasonable request.

References

41. Zhou, Y. F. et al. Improving the molecular ion signal intensity for in situ liquid SIMS analysis. *J. Am. Soc. Mass Spectrom.* **27**, 2006–2013 (2016).
42. Duan, Y. et al. A point-charge force field for molecular mechanics simulations of proteins based on condensed-phase quantum mechanical calculations. *J. Comput. Chem.* **24**, 1999–2012 (2003).
43. Liu, X. H., Han, Y. N. & Yan, T. Y. Temperature effects on the capacitance of an imidazolium-based ionic liquid on a graphite electrode: a molecular dynamics simulation. *ChemPhysChem* **15**, 2503–2509 (2014).
44. Borodin, O. Polarizable force field development and molecular dynamics simulations of ionic liquids. *J. Phys. Chem. B* **113**, 11463–11478 (2009).
45. Hess, B., Kutzner, C., van der Spoel, D. & Lindahl, E. Gromacs 4: algorithms for highly efficient, load-balanced, and scalable molecular simulation. *J. Chem. Theory Comput.* **4**, 435–447 (2008).
46. Bedrov, D., Borodin, O., Li, Z. & Smith, G. D. Influence of polarization on structural, thermodynamic, and dynamic properties of ionic liquids obtained from molecular dynamics simulations. *J. Phys. Chem. B* **114**, 4984–4997 (2010).

Author contributions

Z.Z., C.W. and K.X. conceived the project. Y.Zhou prepared the battery cells. Y.Zhou and X.Y. conducted the in situ liquid-SIMS characterizations. Y.Zhou, Y.Zhang and J.W. organized the SIMS data and drew relevant figures. M.S. and Z.X. performed the MD simulations. Z.Z. and Y.Zhou drafted the manuscript with help from C.W. and K.X.. X.R., R.C. and W.X. provided the relevant chemicals. W.X., D.R.B., Y.D., O.B., Y.W. and X.-L.W. contributed to the discussion and revision of the manuscript.

Competing interests

A US patent (10,505,234 B2) was granted to Battelle Memorial Institute for the protection of the innovation of the liquid battery cell used in this work.

Additional information

Supplementary information is available for this paper at https://doi.org/10.1038/s41565-019-0618-4.

Correspondence and requests for materials should be addressed to K.X., Z.X., C.W. or Z.Z.

Peer review information *Nature Nanotechnology* thanks Bing Joe Hwang and the other, anonymous, reviewer(s) for their contribution to the peer review of this work.

Reprints and permissions information is available at www.nature.com/reprints.